Effective ENSO Amplitude Forecasts Based on Oceanic and Atmospheric Preconditions

ZHUOLIN XUAN,[a] WENJUN ZHANG,[a] FENG JIANG,[a] AND FEI-FEI JIN[b]

[a] *CIC-FEMD/ILCEC, Key Laboratory of Meteorological Disaster of Ministry of Education, Nanjing University of Information Science and Technology, Nanjing, China*

[b] *Department of Atmospheric Sciences, School of Ocean and Earth Science and Technology, University of Hawai'i at Mānoa, Honolulu, Hawaii*

(Manuscript received 16 May 2021, in final form 16 January 2022)

ABSTRACT: Current climate models have relatively high skills in predicting El Niño–Southern Oscillation (ENSO) phase (i.e., El Niño, neutral, and La Niña), once leaping over the spring predictability barrier. However, it is still a big challenge to realistically forecast the ENSO amplitude, for instance, whether a predicted event will be strong, moderate, or weak. Here we demonstrate that the accumulated westerly wind events (WWEs)/easterly wind surges (EWSs) and oceanic recharged/discharged states are both of importance in accurate ENSO amplitude forecasts. El Niño and La Niña events exhibit asymmetric temporal and spatial features in the atmospheric and oceanic preconditions. El Niño amplitude at the peak season is closely associated with the accumulated WWEs over the eastern equatorial Pacific from the previous December to May and the recharged state in the western equatorial Pacific during February. In contrast, the amplitude of La Niña events is sensitive to the accumulated EWSs over the equatorial western Pacific from the previous November to April and the discharged state extending from the equatorial western to central Pacific during February. Considering these asymmetric atmospheric and oceanic preconditions of El Niño and La Niña cases, a statistical model is established to accurately forecast the ENSO amplitude at its mature phase during 1982–2018, which is validated to be robust based on a 1-yr cross-validation and independent sample tests. The feasibility and the limitation of the established statistical model are also discussed by examining its practical utility.

KEYWORDS: Asymmetry; Atmosphere-ocean interaction; ENSO; Statistical forecasting

1. Introduction

El Niño–Southern Oscillation (ENSO), the predominant mode of year-to-year climate variability in the tropical Pacific, arises from large-scale coupled ocean–atmosphere interactions. The ENSO phenomenon has attracted extensive scientific interest and great public attention due to its significant global climate impacts (Wallace et al. 1998; McPhaden et al. 2006; Timmermann et al. 2018). During past few decades, many theories have been proposed to understand the dynamics and potential predictability of ENSO (e.g., Bjerknes 1969; Wyrtki 1975; Cane and Zebiak 1985; Jin 1997a,b; Neelin et al. 1998; Wallace et al. 1998). The rapid development of ENSO during boreal summer and autumn seasons is mainly attributed to the positive ocean–atmosphere feedback first proposed by Bjerknes (1969), emphasizing that the westerly wind anomaly driven by a weakened zonal sea surface temperature (SST) gradient along the equator could further reduce the zonal SST gradient. However, the Bjerknes's positive feedback cannot explain the ENSO phase transition between warm and cold events. Several different mechanisms were proposed to understand the oscillatory nature of ENSO by involving delayed negative feedbacks (Suarez and Schopf 1988; Battisti and Hirst 1989; Cane et al. 1990; Jin 1997a,b; Picaut et al. 1997; Weisberg and Wang 1997). Especially, the recharge oscillator theory highlights the slow ocean adjustment dynamics originated from the imbalance between zonal wind stress and warm water volume (WWV; the volume of water above the 20°C isotherm in the entire equatorial Pacific). The upper heat content in the equatorial Pacific (i.e., WWV) can be used as an effective predictor for ENSO SST since the WWV usually leads the ENSO SST by a quarter of the ENSO period (~6–9 months) (Meinen and McPhaden 2000; McPhaden 2003). However, this phase-lag relationship exhibits a remarkable decadal shift around early 2000s with the lead time being reduced from two to three seasons to one season (Bosc and Delcroix 2008; Horii et al. 2012; McPhaden 2012; Bunge and Clarke 2014), which is closely related to the ENSO regime change with more frequent central Pacific (CP) El Niño events (Zhang et al. 2019; Zhao et al. 2021). Accordingly, the skillful lead time of ENSO prediction has decreased from about two seasons to only one season around 2000 (Hendon et al. 2009; Wang et al. 2010; Zhang et al. 2019). Recently, the upper heat content in the western equatorial Pacific is argued to be a better predictor at a relatively long lead time than that in the whole equatorial Pacific (Lai et al. 2015; Planton et al. 2018; Izumo et al. 2019). For example, one recent study argued that the western Pacific heat content can be identified as an ENSO precondition with a 1-yr lead, which reflects the slow recharge before the spring predictability barrier (Izumo et al. 2019).

As another key precursor of El Niño events, the westerly wind events (WWEs) are a typical atmospheric phenomenon over the equatorial Pacific with the commonly east–west trade winds being shifted to west–east (e.g., Luther et al. 1983; Harrison and Giese 1991; Harrison and Vecchi 1997; Hartten

Corresponding author: Wenjun Zhang, zhangwj@nuist.edu.cn

DOI: 10.1175/JCLI-D-21-0383.1

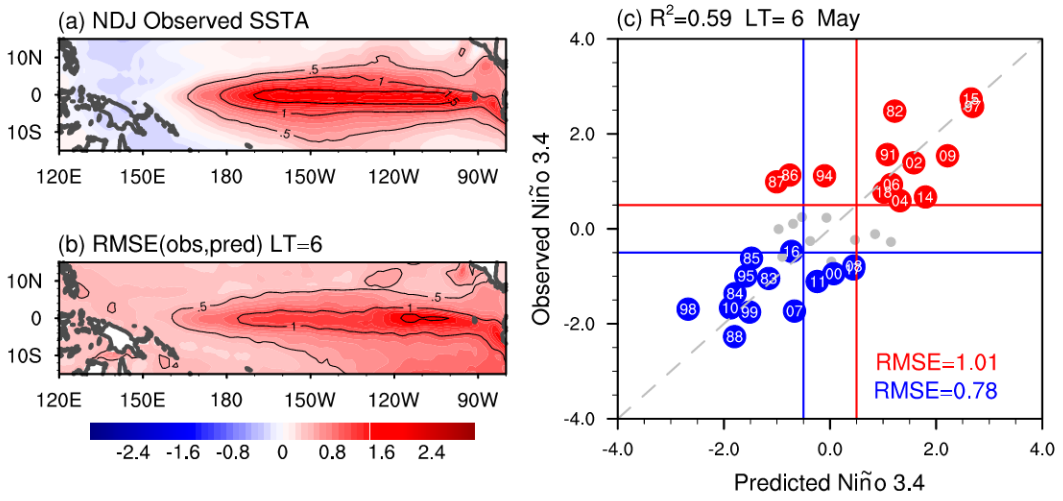

FIG. 1. The composite spatial patterns of (a) observed NDJ SST anomalies and (b) RMSE between the observed and predicted SST anomalies from NCEP CFSv2 at the lead time of 6 months during 1982–2018. The SST anomalies in (a) are calculated as the difference between El Niño and La Niña events divided by 2. (c) Scatterplot between the observed and predicted Niño-3.4$_{NDJ}$ from NCEP CFSv2 for El Niño (red circles), La Niña (blue circles), and neutral (gray circles) years. Numerals in (c) denote the last two digits of the year. The forecast error with respect to the observation for El Niño and La Niña, together with the explained variance (R^2), are shown in (c).

1996; Vecchi and Harrison 2000). The WWEs are initially treated as stochastic atmospheric processes, occurring independently from the ENSO associated dynamics (Battisti and Sarachik 1995; Kleeman and Moore 1997). However, the observation shows that more frequent WWEs are usually accompanied with El Niño events (Eisenman et al. 2005; Seiki and Takayabu 2007; Tziperman and Yu 2007). The WWEs are often proposed to act as a trigger for El Niño onset by stimulating the eastward-propagating downwelling Kelvin wave and suppressing the thermocline in the central and eastern equatorial Pacific (e.g., McPhaden and Yu 1999; Boulanger et al. 2001; Lengaigne et al. 2004; Fedorov et al. 2015). Recent observed and simulated analyses demonstrated that the WWEs can also contribute to the diverse characteristics of El Niño events (Eisenman et al. 2005; Jin et al. 2007; Lian et al. 2014; Chen et al. 2015). Similarly, the eastward counterpart to the WWEs, known as the easterly wind surges (EWSs), were claimed to be important for the onset and development of La Niña (Chiodi and Harrison 2015). Observational evidence shows that the WWEs and EWSs exhibit several asymmetric features, such as zonal extension (Puy et al. 2016) and frequency of occurrence (Hayashi and Watanabe 2016). The basic characteristics of WWEs and EWSs and their relationship with ENSO has been extensively studied, although the root causes of these wind bursts are still debated (Chang et al. 1979; Keen 1982; Love 1985; Nitta 1989; Lander 1990; Chiodi et al. 2014; Puy et al. 2016).

Over the past few decades, ocean data assimilation and atmospheric convection schemes have been developed to improve the capability of dynamical models to predict the ENSO evolution (e.g., Xue et al. 2011; Zhu et al. 2012, 2017; Guilyardi et al. 2004; Neale et al. 2008; Watanabe et al. 2011). State-of-the-art dynamical models can realistically predict the ENSO events 3–6 months in advance. Several statistical models have also been developed for ENSO prediction by involving oceanic heat content and atmospheric preconditions, outperforming some dynamical models (e.g., Tseng et al. 2017; Fang and Mu 2018; Lai et al. 2018; Chiodi 2019). Current dynamical and statistical models both have a relatively good ability to predict the phase of ENSO (i.e., El Niño, La Niña, and neutral), once leaping over the spring predictability barrier. However, it is still a great challenge to predict the ENSO amplitude at its peak phase accurately by using either the dynamical or statistical models. As an example, the forecast at the lead time of 6 months from the Coupled Forecast System, version 2 (CFSv2), of the National Centers for Environmental Prediction (NCEP), could explain about 60% of the total variance for the observed ENSO variability (measured as the Niño-3.4 index; Fig. 1c) at the mature phase, suggesting the relative high skill of CFSv2 to predict ENSO phase. However, it exhibits large root-mean-square error (RMSE) respective to the observation, about two-thirds of the observed ENSO SST magnitude in the tropical central to eastern Pacific (Fig. 1). The 6-month lead forecast error versus the observation is about 1.01°C for El Niño and 0.78°C for La Niña, respectively. Accordingly, the ENSO amplitude in the mature winter might be largely overestimated or underestimated in the 6-month-lead prediction. Due to the difficulty in forecasting the ENSO amplitude, the Climate Prediction Center (CPC) provides the probability of ENSO phases rather than the explicit ENSO amplitude information (Tippett et al. 2019). So far, the ENSO amplitude forecast at its peak still remains a big challenge and the decisive atmosphere–ocean preconditions are not clear, although numerous studies have suggested the importance of oceanic and atmospheric preconditions on the ENSO development (e.g., Meinen and

McPhaden 2000; McPhaden 2003; Lengaigne et al. 2004; Fedorov et al. 2015; Chen et al. 2015). The ENSO amplitude forecasts at the 6-month lead deserve attention for better regional disaster prevention and mitigation due to distinct climate impacts for different ENSO amplitudes (e.g., Lyon 2004; Lyon and Barnston 2005; Hoell et al. 2016; Geng et al. 2017).

In this study, we focus on the accurate prediction of ENSO amplitude at its mature phase on the grounds of the previous physical understanding in ENSO dynamics as well as the great efforts in ENSO prediction. El Niño and La Niña events are separately considered to examine their respective oceanic and atmospheric preconditions, since they show highly asymmetric features (e.g., Jin et al. 2003; Ohba and Ueda 2007; Zhang et al. 2009; Okumura and Deser 2010; Chen et al. 2016). We first examine the linkage of ENSO amplitude with the preceding atmospheric and oceanic conditions and explore possible effective precursors of ENSO amplitude during its peak phase. A statistical forecast model is then established in consideration of asymmetric atmospheric and oceanic preconditions. We also examine the practical utility of the established model and clarify its feasibility and limitation. We demonstrate that ENSO amplitude at its mature phase can be well predicted at the lead time of 6 months under the premise of the accurate ENSO phase prediction.

The paper is structured as follows. Section 2 describes the data and method used in this study. Section 3 investigates the asymmetric atmospheric and oceanic preconditions for El Niño and La Niña cases, respectively. Next, the statistical model for the ENSO amplitude forecasts and its validation are presented in section 4. Section 5 shows the feasibility and the limitation of the constructed model by examining its practical utility. Finally, the main conclusion and discussion are summarized in section 6.

2. Data and methodology

The monthly SST datasets used in the study are derived from version 2 of the National Oceanic and Atmospheric Administration (NOAA) optimum interpolation (OI) SST analysis (Reynolds et al. 2002). The upper ocean heat content is examined based on oceanic subsurface potential temperature from the NCEP Global Ocean Data Assimilation System (GODAS; Behringer and Xue 2004). The daily averaged zonal wind at 10-m altitude is obtained from the European Centre for Medium-Range Weather Forecasts (ECMWF) interim reanalysis dataset (ERA-Interim; Dee et al. 2011). This dataset, closely matched to the Tropical Atmosphere Ocean (TAO) observation (Chiodi and Harrison 2015), is widely used in the studies of high-frequency wind burst (e.g., Puy et al. 2016; Chen et al. 2017; Capotondi et al. 2018; Shi and Su 2020; Liang et al. 2021). Monthly SST forecasts in the tropical Pacific are provided by the Coupled Forecast System (CFSv2) of the NCEP (more information available online at http://cfs.ncep.noaa.gov/). The analyses cover the period of 1982–2018. The spatial resolution is 1° × 1° for the SST and upper heat content and 0.5° × 0.5° for the 10-m wind. All anomalies are computed by removing the climatology in the entire period.

TABLE 1. ENSO events for the 1982–2018 period.

ENSO phase	Years
El Niño	1982/83, 1986/87, 1991/92, 1994/95, 1997/98, 2002/03, 2004/05, 2006/07, 2009/10, 2015/16, 2018/19
La Niña	1983/84, 1988/89, 1995/96, 1998/99, 2007/08, 2010/11, 2016/17

ENSO events are defined when the 3-month running-mean Niño-3.4 index (averaged SST anomaly in the region of 5°S–5°N, 120°–170°W) is above the threshold of ±0.5°C for 5 consecutive months, consistent with the CPC's definition. The ENSO events during 1982–2018 are listed in Table 1. Months labeled "(0)" and "(−1)" denote months of ENSO developing year and the preceding year, respectively. Since the peak phase of ENSO in observations tends to occur in boreal winter (Rasmusson and Carpenter 1982), the ENSO peak amplitude is measured as the winter [November–January (NDJ)] Niño-3.4 index. Qualitative conclusion remains the same if the season for calculating the peak amplitude slightly changes. It is worth mentioning that the second-year and third-year La Niña events are not considered here due to their complicated initiation mechanism (e.g., Ohba and Ueda 2007, 2009; Okumura and Deser 2010; Dommenget et al. 2013). A 90-day high-pass Lanczos filter is applied to obtain the high-frequency zonal wind (U_{hf}). According to the previous definition (Chen et al. 2017), we define the WWEs-index (EWSs-index) as the exceeding part of the high-frequency zonal wind greater (less) than positive (negative) one standard deviation for each grid point. Then, the accumulated WWEs-index (EWSs-index) can be obtained through integrating the WWEs-index (EWSs-index) for a certain region in a particular period:

$$\text{Accu} - \text{WWEs} = \int\int \text{WWE} - \text{index}\, dSdT, \tag{1}$$

$$\text{Accu} - \text{EWSs} = \int\int \text{EWS} - \text{index}\, dSdT, \tag{2}$$

where S indicates the area and T indicates the period. The oceanic state of heat content is approximately measured as the subsurface potential temperature anomaly (PTA) averaged from 5 to 250 m. Considering important effects of wind on PTA, we use the linearly dependent PTA anomalies from the surface wind to detect the decisive regions of El Niño and La Niña for their amplitudes, respectively. Note that we construct the statistical model for ENSO amplitude by using the original PTA anomalies for simplicity considering the linearity in the multiregression.

3. Asymmetric atmospheric and oceanic precondition to ENSO

a. Asymmetric accumulated WWEs/EWSs

We characterize the composite SST tendency of El Niño and La Niña events by using the derivative of the Niño-3.4 index (dNiño3.4/dt) in Fig. 2. For El Niño, the SST tendency

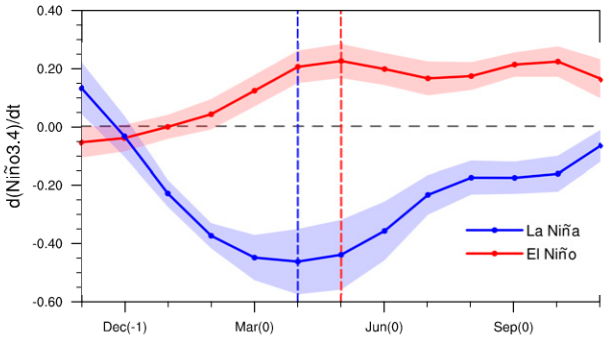

FIG. 2. Composite monthly evolution of the time derivative of Niño-3.4 (dNiño3.4/dt; °C month^{-1}) smoothed by a three-point running mean for El Niño (red line) and La Niña (blue line). The shading represents one standard deviation for composite El Niño (red shading) and La Niña (blue shading) years. Numerals "−1" and "0" in parentheses along the abscissa denote the year before and during the ENSO development, respectively. The red and blue dashed lines indicate the peak of the El Niño and La Niña developing rate, respectively.

exhibits two peaks during the developing spring and autumn, respectively. The developing rate during autumn is not discussed in this study, since the precondition at the lead time of at least 6 months is our focus. In contrast, the developing rate of La Niña reaches its peak during April, leading that of El Niño by about 1 month. The timing difference of their developing rate could be related to the distinct oceanic state and atmospheric conditions. Considering the oceanic heat content evolution of El Niño and La Niña are relatively symmetric in terms of the timing (not shown), the timing difference between El Niño and La Niña (Fig. 2) could be associated with their asymmetric zonal wind conditions. As shown in previous studies, two main pathways are involved for high-frequency wind burst to influence the ENSO development, one of which is the thermocline feedback through upwelling of anomalous subsurface temperature, and the other of which is the zonal advection feedback through anomalous zonal current transport (e.g., McPhaden and Yu 1999; Lengaigne et al. 2003, 2004; Fedorov et al. 2015). These oceanic feedbacks dominantly contribute to the ENSO growth rate, which is the key factor to measure the ENSO amplitude (Jin 1997a,b; Jin et al. 2006). We here use the 6-month integration for the WWEs from December(−1) to May(0) and the EWSs from November(−1) to April(0) to roughly represent the accumulated effect of the high-frequency wind associated with El Niño and La Niña, respectively. It is notable that the developing rate of La Niña is stronger than that of El Niño in the developing spring (near ENSO onset time), which could be explained by the observed fact that first-year La Niña events are usually preconditioned with El Niño while the El Niño years are often preceded by neutral state on average (e.g., Kessler 2002; Larkin and Harrison 2002; Fang and Yu 2020).

To investigate the possible asymmetric features in zonal distribution of accumulated WWEs/EWSs, Fig. 3 shows the diversity of zonal distribution of high-frequency zonal wind burst accumulated from 120°E to the indicated longitude for all El Niño and La Niña events. Here, the accumulated zonal wind starting from 120°E is used to detect the integrated effects of wind from the western to eastern equatorial Pacific. The accumulated WWEs for El Niño display a large spread from the central to eastern equatorial Pacific; in contrast,

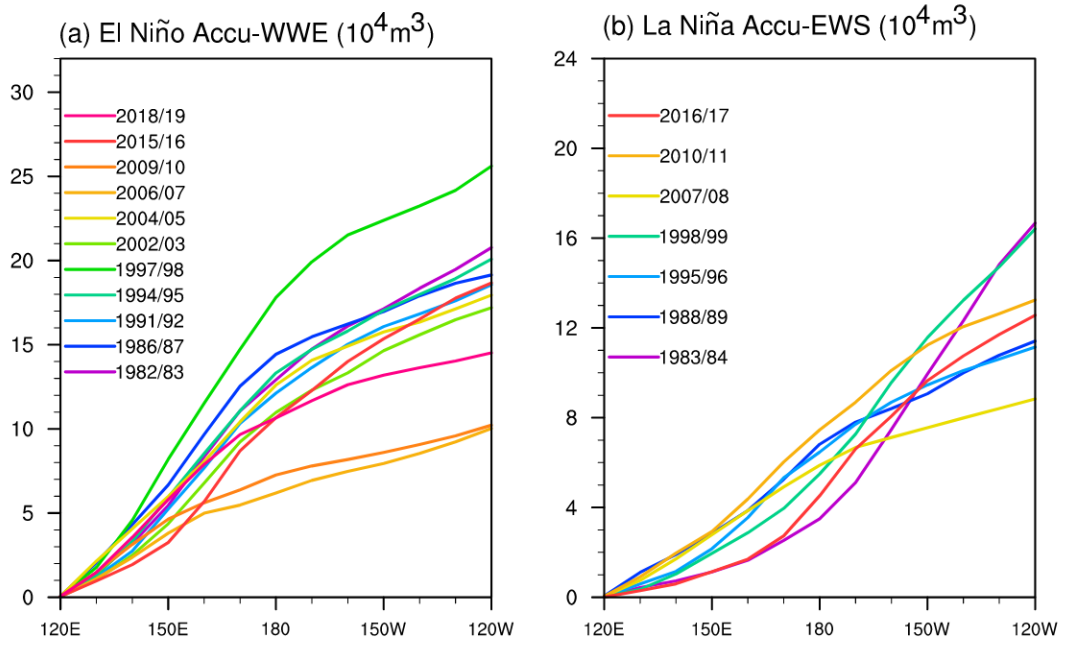

FIG. 3. (a) The zonal distributions of accumulated WWEs for all El Niño events from December(−1) to May(0) over a sliding region. The meridional extent is 5°S to 5°N, and the zonal extent is 120°E to the indicated longitude. (b) As in (a), but for November(−1)–April(0) accumulated EWSs for La Niña events.

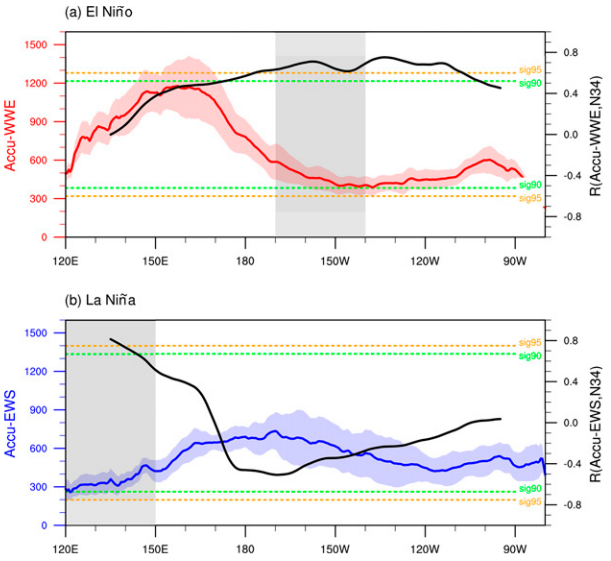

FIG. 4. (a) Composite zonal patterns of December(−1) to May(0) accumulated WWEs (red line; m s^{-1}) and correlation coefficient (black line) between the Niño-3.4$_{NDJ}$ and the accumulated WWEs within a 30°-longitude running window for El Niño. (b) Composite zonal patterns of November(−1) to April(0) accumulated EWSs (blue line; m s^{-1}) and correlation (black line) between the Niño-3.4$_{NDJ}$ and the accumulated EWSs within a 30°-longitude running window for La Niña (blue line). The red and blue shading represents one standard deviation of the preceding WWEs for El Niño and EWSs for La Niña, respectively. The gray boxes denote the corresponding longitude ranges of accumulated WWEs/EWSs with maxima correlation coefficient. The green and orange dashed lines represent the 90% and 95% significance levels, respectively.

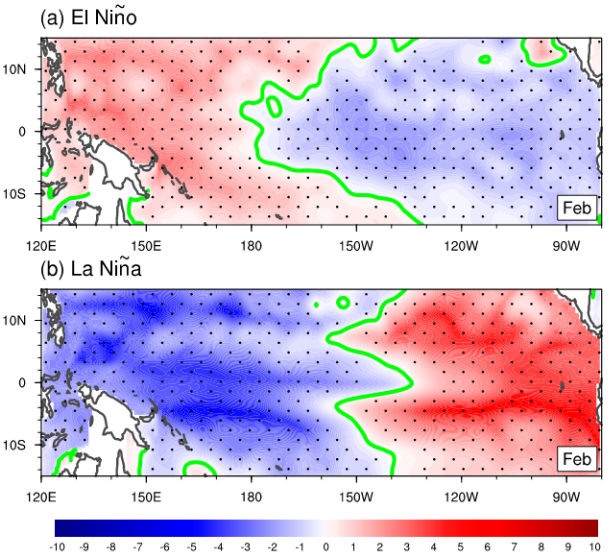

FIG. 5. Composite spatial distributions of the potential temperature anomalies (shading; °C) averaged over 5–250 m during the February(0) of (a) El Niño and (b) La Niña years. The green lines denote zero values. Dots indicate composite values above the 99% significance level.

those in the western Pacific are relatively not easy to be well distinguished. The WWEs for some El Niño events, such as 2006/07 and 2009/10 events, are confined in the western equatorial Pacific and that for some El Niño events, such as 1982/83 and 1997/98 events, can extend to the eastern equatorial Pacific (Fig. 3a). Different from El Niño, La Niña events show a large spread in the EWSs almost over the entire equatorial Pacific (Fig. 3b). In general, the preceding WWEs for El Niño is stronger than the EWSs for La Niña (Fig. 4), which could be associated with the variables used (e.g., Chiodi and Harrison 2015; Puy et al. 2016). To explore the high related region with the ENSO amplitude, we in Fig. 4 also show the zonal correlation pattern of the boreal winter Niño-3.4 index with the accumulated WWEs/EWSs within a 30°-longitude running window. For El Niño, the maximum correlation (~0.7) appears in the central and eastern equatorial Pacific around 140°–170°W, different from the largest magnitude of WWEs occurring the western equatorial Pacific (Fig. 4a). The accumulated WWEs in the region east of the strongest WWE can be identified as a good indicator of the eastward extension of the WWEs. We show that the El Niño amplitude at the mature phase is sensitive to the zonal extension of WWEs, consistent with previous studies that the farther eastward expansion of WWEs could lead to the farther eastward extended warm pool and favor stronger El Niño (Lengaigne et al. 2003; Eisenman et al. 2005; Vecchi 2006; Gebbie et al. 2007). Likely for La Niña, the accumulated EWSs are strongest in the central Pacific; however, the correlation between the La Niña amplitude and accumulated EWSs is the strongest (~0.8) around 120°–150°E (Fig. 4b). The accumulated EWSs in the region west of the strongest EWSs can well measure the westward extension of the EWSs, suggesting that the farther westward extension of EWSs tend to favor a stronger La Niña via the farther westward extension of the warm pool. The above analyses show that the different preceding high-frequency zonal winds of warm and cold episodes, in terms of the timing and region, are closely associated with their amplitudes at the peak phase. The WWEs over 140°–170°W from December(−1) to May(0) and the EWSs over 120°–150°E from November(−1) to April(0) could play an important role in determining El Niño and La Niña amplitudes, respectively.

b. *Asymmetric oceanic recharged/discharged states*

Previous studies have shown that the upper heat content in the western equatorial Pacific during February (0) is crucial for the ENSO development and thus the optimal choice for ENSO prediction (e.g., Lai et al. 2015, 2018). In this study, the February(0) heat content anomaly is also used as the preceding oceanic signal following Lai et al. (2018). Figure 5 shows the 5–250-m averaged PTA in February(0) for the El Niño and La Niña composites, respectively. Here we exclude the interference of the accumulated high-frequency zonal wind (i.e., accumulated WWEs/EWSs in section 3a) from the upper heat content anomalies by linear regression to consider the role of the oceanic process independent of the accumulated WWEs/EWSs. During February(0) for the El Niño composite, the positive upper heat content anomalies occur west of

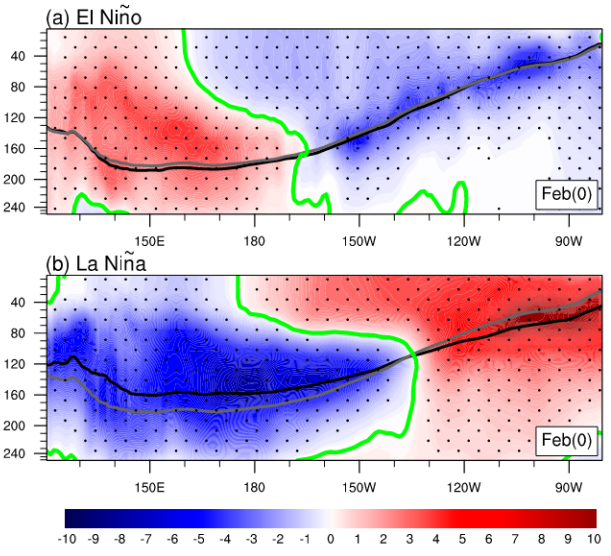

FIG. 6. Composite potential temperature anomalies (shading; °C) averaged along the equator (5°S–5°N) during the February(0) of the (a) El Niño and (b) La Niña years. The climatological (gray line) and anomalous 20°C isotherms (black line) are also displayed. The green lines denote zero values. Dots indicate composite values above the 99% significance level.

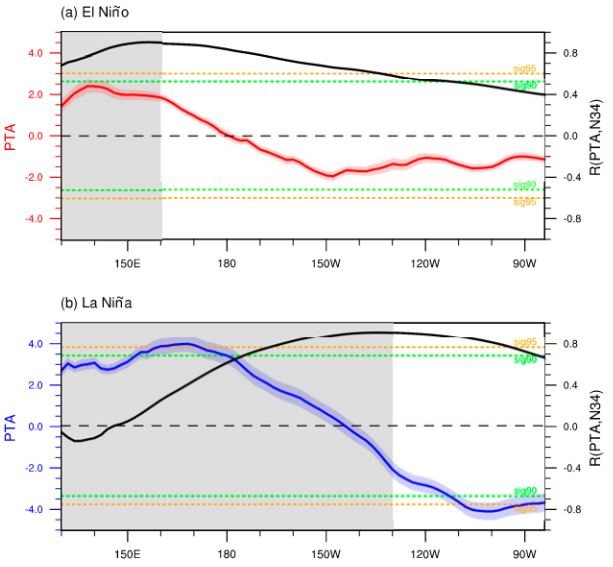

FIG. 7. (a) Composite zonal distributions of PTA (red line) averaged over 5–250 m along the equatorial Pacific (5°S–5°N, 130°E–80°W) during February(0) of El Niño and correlation coefficient (black line) between the Niño-3.4$_{NDJ}$ and the PTA integrating from 130°E to the indicated longitude. (b) As in (a), but for La Niña (blue line). The red and blue shading represents one standard deviation for the preceding PTA for El Niño and La Niña, respectively. The gray boxes denote the corresponding longitude ranges of PTA with the maxima correlation coefficient. The green and orange dashed lines represent the 90% and 95% significance levels, respectively.

the date line, and the negative anomalies cover most of the central and eastern equatorial Pacific (Fig. 5a). The composite upper heat content for La Niña exhibits negative and positive anomalies west and east of 150°W, respectively (Fig. 5b). Different oceanic preconditions for El Niño and La Niña can also be observed in the longitude–depth PTA distribution along with the 20°C isothermal depth (D20) at the equatorial Pacific (Fig. 6). For El Niño, the preceding recharged state over the western Pacific corresponds to the deepening thermocline west of the date line, while during La Niña the thermocline depth west of 130°W greatly shallows as compared to the climatology, consistent with the upper heat content anomalies. After removing the effects of highly asymmetric high-frequency wind, it appears that the strength and zonal extension of the PTA are both smaller for the recharged state of El Niño than those for the discharged state of La Niña. The asymmetric features in the intensity of the PTA are also shown in the recharge–discharge process for ENSO (e.g., Ohba and Ueda 2007; An and Kim 2018), which are further magnified by removing the counteracting effects of high-frequency wind. The differences in the zonal extension of the PTA might be related to the different zonal extensions of WWE and EWS.

We then show in Fig. 7 the zonal correlation pattern of the boreal winter Niño-3.4 index with the linearly independent PTA integrating from 130°E to the indicated longitude to explore the key PTA region associated with the ENSO amplitude. Note that the interference of the atmospheric factor (i.e., accumulated WWE/EWS index in section 3a) is also linearly regressed out from the sea surface temperature to determine to what extent the PTA explains the residual part of ENSO amplitude. The same conclusion can also be obtained by using the original ENSO amplitude with a relatively reduced correlation due to interference from the surface wind. Corresponding to the zonal extension of the recharged state, the El Niño amplitude has the highest correlation (~0.9) with the PTA integrating from 130° to 160°E (Fig. 7a). In contrast, the La Niña amplitude has the maximum correlation (~0.9) with the PTA integrating from 130°E to 130°W (Fig. 7b). Similar to the preconditioning high-frequency zonal wind of El Niño and La Niña, the preceding oceanic recharged and discharged states in association with ENSO amplitudes in the peak phase also exhibit asymmetric features.

4. Statistical model for ENSO amplitude forecasts and its validation

Previous statistical and dynamical models have shown a relatively high predictive skill of ENSO phases (e.g., Tseng et al. 2017; Fang and Mu 2018; Lai et al. 2018; Chen et al. 2020; Zhu et al. 2012, 2017). On this basis, we make further efforts to realistically predict the ENSO amplitudes at the peak phase. Our analyses documented that the atmospheric and oceanic preconditions of El Niño and La Niña exhibit highly asymmetric features in both timing and spatial pattern. It suggests that we should consider El Niño and La Niña events separately when developing the statistical model for the ENSO amplitude forecast. The statistical model is established by

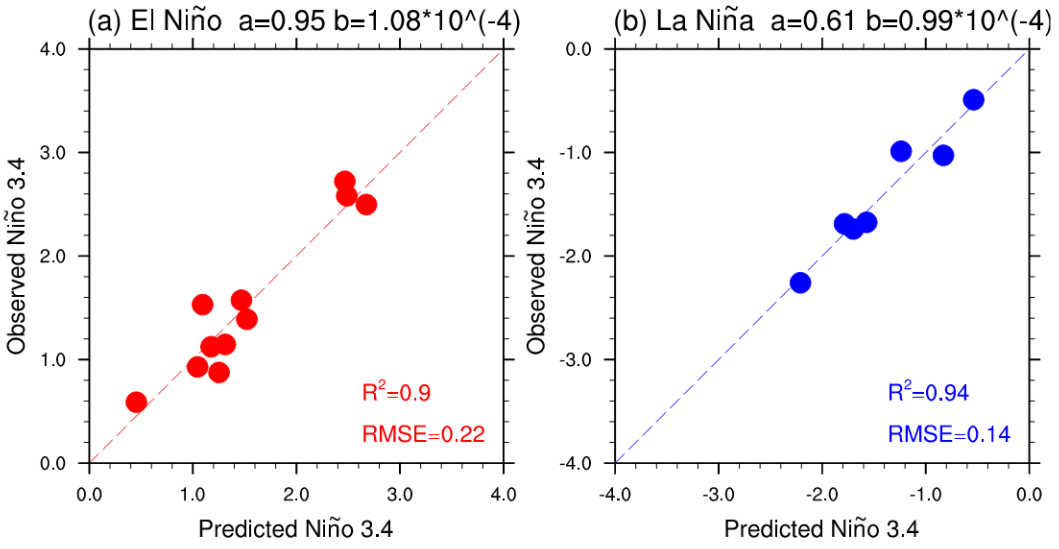

FIG. 8. (a) Scatterplot of the observed and predicted Niño-3.4$_{NDJ}$ based on the statistical model during El Niño years. (b) As in (a), but for La Niña. The coefficients (a and b) are shown above each plot. The RMSE and R^2 are also displayed.

considering the combined effect of preceding oceanic recharged/discharged state (θ) and atmospheric accumulated WWEs/EWSs $\left(\sum_i U_{\mathrm{WWE/EWS}}\right)$:

$$\mathrm{Niño3.4_{NDJ}} = a\theta + b\sum_i U_{\mathrm{WWE/EWS}}. \quad (3)$$

For the El Niño model, the expected winter Niño-3.4 SST anomaly is computed using the linear method based on two parameters: the 130°–160°E PTA during February(0) and the accumulated 140°–170°W WWEs from December(−1) to May(0). In the La Niña model, two parameters used are the 130°E–130°W PTA in February(0) and the accumulated 120°–150°E EWSs from November(−1) to April(0). The coefficients (a and b) are determined by least squares fitting over the training period. All the periods and domains are selected based on the analyses in section 3. For simplicity, the original PTA anomalies are used to construct the statistical model for ENSO amplitude due to the linearity in the multi-regression. We tested the R^2 (explained variance; R is the correlation coefficient) between the predicted and observed ENSO amplitude by slightly varying the season and domain, and our parameters selected result into the best performance. Note that the February recharged/discharged state was selected as the oceanic precondition following the previous study (Lai et al. 2018). We also tested R^2 between the predicted and observed ENSO amplitude by varying the month of PTA from February to May, and February was found to be the optimal choice with the maximum R^2 (not shown).

Figure 8 displays the scatterplot of the predicted and observed Niño-3.4$_{NDJ}$ for El Niño and La Niña events, respectively. In the hindcast model of El Niño amplitude for the full period, the preceding PTA and accumulated WWEs at the lead time of six months can explain about 90% of the total variance in the Niño-3.4$_{NDJ}$ SST anomaly and the RMSE between the prediction and observation is 0.22°C (Fig. 8a). The accumulated WWEs alone can explain about 49% of the total variance, and the oceanic heat content can explain 80% of the rest variance (not shown). As for La Niña, about 94% of the total variance can be explained by the preceding PTA and accumulated EWSs, and the corresponding RMSE is about 0.14°C (Fig. 8b). About 64% of the total variance can be explained by the accumulated EWSs, and the oceanic heat content can explain 81% of the rest variance. Overall, our established statistical model is capable of accurately capturing the amplitude of the observed ENSO events.

Due to the limited sample size, a 1-yr cross validation is further applied to test overfitting of our model following previous studies (e.g., Clarke and Gorder 2003; Lai et al. 2018). The model is cross-validated by training the model over all of the El Niño/La Niña years except for 1 year being tested. When excluding any one El Niño/La Niña year from the training periods, the explained variance is always greater than 85% and the RMSE is always below 0.25°C (Fig. 9), suggesting high stability for the model. The corresponding coefficients (a and b) for the 1-yr cross validation are shown in Table 2. The coefficients are similar to the full hindcast model and not sensitive to the specific training samples. For example, the coefficient a for La Niña is 0.61 in the full hindcast model and ranges from 0.51 to 0.72 for 1-yr cross validation.

In addition to the 1-yr cross validation, we divided the 18 ENSO years during 1982–2018 into two subsets of the former 14-yr and latter 4-yr samples or the former 12-yr and latter 6-yr samples. The former samples are used to train the model and compute the coefficients. The latter are used for hindcasting as the independent sample test. For the independent four ENSO years, the R^2 and the RMSE between the predicted and observed amplitude are 96% and 0.34°C, respectively (Fig. 10a). If we increase the hindcasting periods to 6 years,

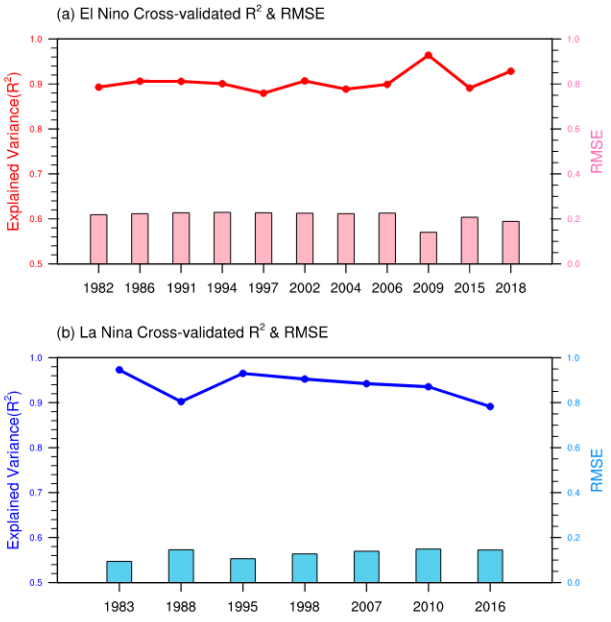

FIG. 9. The magnitude of R^2 (lines) and RMSE (bars) for every indicated (a) El Niño and (b) La Niña year cross validated.

the R^2 and the RMSE are 97% and 0.33°C, respectively (Fig. 10b). Despite very limited samples for the ENSO events, the established statistical model is validated to be robust in the current period based on a 1-yr cross validation and different independent sample tests.

5. Practical utility of the established model

A robust statistical model for ENSO amplitude prediction has been established using the effective atmospheric and oceanic precursors. To further examine the performance of our model in practice, we apply the model to practical prediction based on the phases predicted by the NCEP CFSv2. Here we calculated the Niño-3.4$_{NDJ}$ of all years that have been predicted as El Niño or La Niña in the 6-month lead based on our statistical forecast model (Fig. 11b). Targeted on the inconsecutive ENSO events which are correctly predicted in phase, our model can provide much more accurate prediction of ENSO amplitude, showing a better performance respective to the CFS's prediction (Fig. 11). The RMSE between the prediction and observation is 0.22° and 0.13°C for El Niño and La Niña with correct phase prediction, respectively. It is noted that a more objective way to quantify the practical utility is based on all predicted ENSO years. We also show in Fig. 11 the RMSE for all predicted ENSO years including both correctly and falsely predicted events. The RMSE for all predicted El Niño years is comparable to that of the CFSv2 prediction. For all predicted La Niña years, the RMSE of our model is even larger than that of the CFSv2 prediction. It can be appreciated considering that our model cannot work for the falsely predicted ENSO events (two for El Niño events and six for La Niña events), which again emphasizing the importance of correct phase prediction.

For those years predicted to be warm or cold ENSO phases ending up with opposite phases or neural states, our amplitude forecast could not add more useful information. These events could be strongly disturbed by the extratropical noise in the mid- and late-year (e.g., Su et al. 2014; Yu and Fedorov 2020). In this view, the correction of the amplitude prediction for these aborted events based on the oceanic and atmospheric preconditions before June is essentially of little significance. In addition, the predicted amplitude of a second or third year of consecutive La Niña event with correct phase prediction is overestimated to a great extent by our model since its initiation mechanism may be fundamentally different from the first-year event (e.g., Ohba and Ueda 2007, 2009; Okumura and Deser 2010; Dommenget et al. 2013). The accumulated EWSs from November(−1) to April(0) for the second- or third-year event might be considered as an accompaniment of the first-year event, instead of its important precondition. Our statistical model does not apply to these events and further investigation is warranted to find the preconditions associated with the amplitude of these ENSO years. Besides, it is noted that the 1994/95 El Niño was predicted to be neutral in the 6-month lead and thus not included to examine the practical utility.

Overall, the practical utility of our model in predicting the ENSO amplitude relies on the phase prediction skill of current models. Nevertheless, it is encouraging that the NCEP CFSv2 dynamical model succeeded in predicting most ENSO years

TABLE 2. The optimized coefficients (a and b) for 1-yr cross validation.

El Niño years	a_{El} (°C °C^{-1})	b_{El} (10^{-4} °C m^{-3})	La Niña years	a_{La} (°C °C^{-1})	b_{La} (10^{-4} °C m^{-3})
1982/83	1.04	1.16	1983/84	0.56	1.12
1986/87	0.95	1.08	1988/89	0.53	0.98
1991/92	0.97	1.09	1995/96	0.51	0.99
1994/95	0.94	1.08	1998/99	0.72	1.12
1997/98	0.92	1.06	2007/08	0.60	1.02
2002/03	0.94	1.09	2010/11	0.58	1.03
2004/05	1.03	1.14	2016/17	0.54	0.97
2006/07	0.97	1.07			
2009/10	0.83	1.15			
2015/16	0.94	1.01			
2018/19	0.99	1.06			

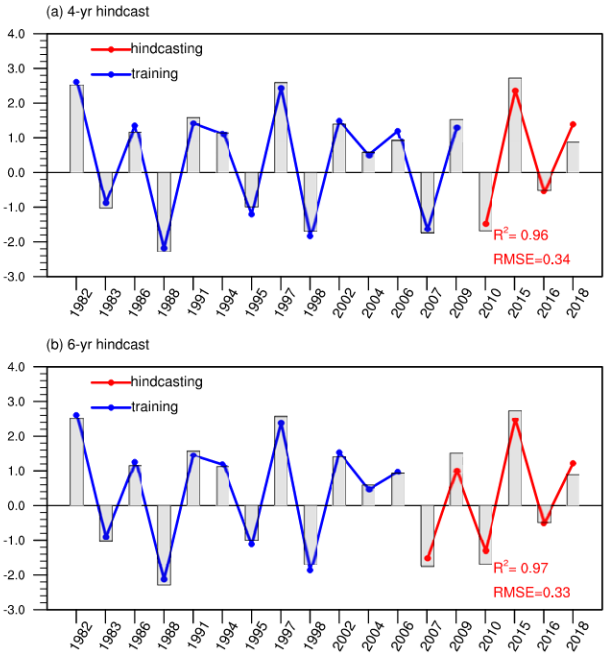

FIG. 10. The magnitude of observed (gray bars) and the statistical model fitted (lines) Niño-3.4$_{NDJ}$ for ENSO years in the (a) 4- and (b) 6-yr hindcasts. The blue lines represent the training results and the red lines the hindcasting results. The R^2 and forecast errors of the hindcasting results are also displayed.

(10 of 13 El Niño and 10 of 14 La Niña) six months in advance during the period of 1982–2018. In the future, as the accuracy of the ENSO phase prediction improves, our model for ENSO amplitude prediction would provide more useful information.

6. Conclusions and discussion

Despite that the current statistical and dynamical models have relatively good skills in predicting ENSO phases, it is still a big challenge to realistically forecast ENSO amplitude at its peak (whether the ENSO event is strong, moderate, or weak). The present study documents that the preceding WWEs/EWSs and oceanic recharged/discharged states both play important roles in determining the ENSO amplitude at the peak period. It is interesting that the atmospheric and oceanic preconditions are highly asymmetric in temporal and spatial features for El Niño and La Niña events. We confirmed the strong influence of the Pacific oceanic heat content and WWEs/EWSs on ENSO in previous studies (e.g., Jin 1997a,b; Meinen and McPhaden 2000; Izumo et al. 2019; Lian et al. 2014; Chen et al. 2015) and found that the El Niño amplitude at its mature phase is closely associated with the western equatorial (5°S–5°N, 130°–160°E) PTA during February(0) and accumulated 140°–170°W WWEs from December(−1) to May(0). In contrast, the La Niña amplitude is sensitive to the western and central equatorial (5°S–5°N, 130°E–130°W) Pacific during February(0) and the accumulated 120°–150°E EWSs from November(−1) to April(0). Considering these asymmetric preconditions, we need to consider El Niño and La Niña events separately to establish their corresponding statistical model for the amplitude forecast. Here, we developed the statistical model based on El Niño and La Niña samples on the basis of correct prediction of ENSO phases in advance. By using the atmosphere–ocean predictions at the lead time of six months, the prediction can explain about 90% of the total variance in the Niño-3.4 SST anomaly during the peak time and the RMSE is less than 0.22°C. Considering that the samples for ENSO events are very limited, our model is

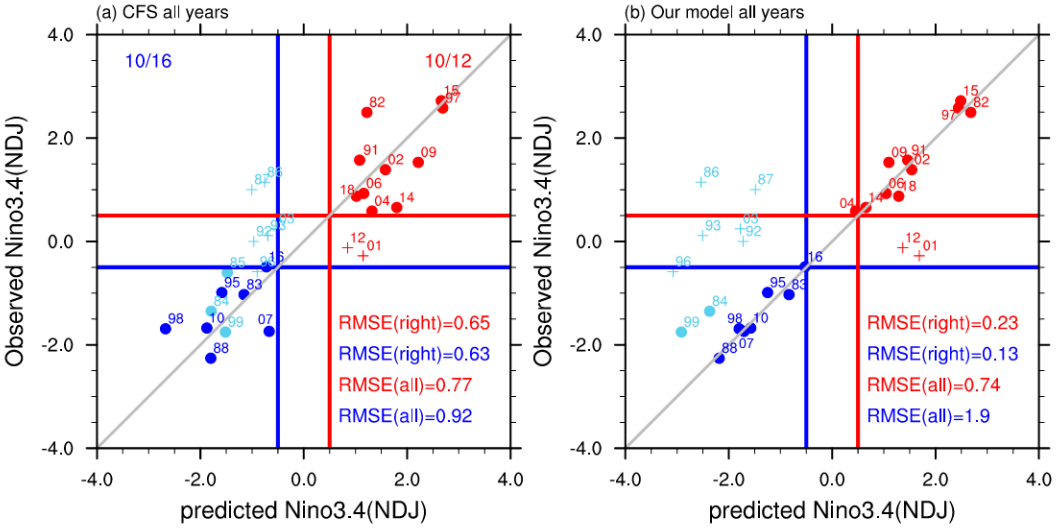

FIG. 11. (a) Scatterplot between the observed and predicted Niño-3.4$_{NDJ}$ for all years that are predicted to be ENSO 6 months in advance based on the NCEP CFSv2 model. (b) Scatterplot between the observed and predicted Niño-3.4$_{NDJ}$ by our statistical model. Circles and crosses denote the correctly and falsely predicted El Niño (red) and La Niña (blue; dark blue for single-year event and light blue for second- or third-year event), respectively. The forecast error of all predicted ENSO years and the correctly predicted ENSO years are also displayed.

validated to be robust using a 1-yr cross validation and different independent sample tests.

Physical mechanisms explaining the high-frequency zonal wind and oceanic state driving the ENSO onset and development have been demonstrated in numerous previous studies (e.g., Jin 1997a,b; Meinen and McPhaden 2000; McPhaden 2003; Izumo et al. 2019; McPhaden and Yu 1999; Boulanger et al. 2001; Lengaigne et al. 2004; Fedorov et al. 2015). Based on these researches, we established the ENSO amplitude forecast model by considering the optimal atmosphere–ocean preconditions separately for El Niño and La Niña events from a statistical standpoint. Our statistical model is constructed based on the data from 1980 to 2018 with limited samples. The different independent sample tests suggest that this configuration is stable under the background change around 2000s due to decadal change or global warming, which increases our confidence for the feasibility of our model. Despite robustness for our model in the current period, its performance needs future samples to be further consolidated.

Based on the conventional theory of ENSO cycle, the favorable oceanic and atmospheric conditions for ENSO before summer are generally followed by significant ENSO SST anomalies in winter. Most of ENSO events are featured with regular evolution and their phase can be correctly predicted at the 6-month lead (Fig. 11a). For these inconsecutive ENSO events with correct phase prediction, our constructed model can provide much more accurate amplitude prediction based on different atmospheric and oceanic preconditions for El Niño and La Niña, respectively. The limitation about the established model should also be noted here. As we have discussed in section 5, the practical utility of our amplitude forecast model is limited to the phase prediction skill of current models. The inaccuracy in phase prediction might be associated with the forecast error including model error and initial condition errors (Goswami and Shukla 1991; Latif et al. 1998; Chen et al. 1995, 2004), or the fact that more information about the following evolution in the mid and late-year are needed for some years such as 2012/13 (Su et al. 2014; Yu and Fedorov 2020). A promising role of the ENSO amplitude prediction model would be anticipated as dynamical models show enhanced prediction skill in phase prediction with the development of physical process simulation and data assimilation methods.

Acknowledgments. This work was supported by the National Nature Science Foundation of China (42088101, 42125501).

REFERENCES

An, S.-I., and J.-W. Kim, 2018: ENSO transition asymmetry: Internal and external causes and intermodel diversity. *Geophys. Res. Lett.*, **45**, 5095–5104, https://doi.org/10.1029/2018GL078476.

Battisti, D. S., and A. C. Hirst, 1989: Interannual variability in a tropical atmosphere–ocean model: Influence of the basic state, ocean geometry, and nonlinearity. *J. Atmos. Sci.*, **46**, 1687–1712, https://doi.org/10.1175/1520-0469(1989)046<1687:IVIATA>2.0.CO;2.

——, and E. S. Sarachik, 1995: Understanding and predicting ENSO. *Rev. Geophys.*, **33**, 1367–1376, https://doi.org/10.1029/95RG00933.

Behringer, D., and Y. Xue, 2004: Evaluation of the Global Ocean Data Assimilation system at NCEP: The Pacific Ocean. *Eighth Symp. on Integrated Observing and Assimilation Systems for Atmosphere, Oceans, and Land Surface*, Washington, DC, Amer. Meteor. Soc., 2.3, https://ams.confex.com/ams/84Annual/techprogram/paper_70720.htm.

Bjerknes, J., 1969: Atmospheric teleconnections from the equatorial Pacific. *Mon. Wea. Rev.*, **97**, 163–172, https://doi.org/10.1175/1520-0493(1969)097<0163:ATFTEP>2.3.CO;2.

Bosc, C., and T. Delcroix, 2008: Observed equatorial Rossby waves and ENSO-related warm water volume changes in the equatorial Pacific Ocean. *J. Geophys. Res.*, **113**, C06003, https://doi.org/10.1029/2007JC004613.

Boulanger, J.-P., and Coauthors, 2001: Role of non-linear oceanic processes in the response to westerly wind events: New implications for the 1997 El Niño onset. *Geophys. Res. Lett.*, **28**, 1603–1606, https://doi.org/10.1029/2000GL012364.

Bunge, L., and A. J. Clarke, 2014: On the warm water volume and its changing relationship with ENSO. *J. Phys. Oceanogr.*, **44**, 1372–1385, https://doi.org/10.1175/JPO-D-13-062.1.

Cane, M. A., and S. E. Zebiak, 1985: A theory for El Niño and the Southern Oscillation. *Science*, **228**, 1085–1087, https://doi.org/10.1126/science.228.4703.1085.

——, M. Münnich, and S. F. Zebiak, 1990: A study of self-excited oscillations of the tropical ocean–atmosphere system. Part I: Linear analysis. *J. Atmos. Sci.*, **47**, 1562–1577, https://doi.org/10.1175/1520-0469(1990)047<1562:ASOSEO>2.0.CO;2.

Capotondi, A., P. D. Sardeshmukh, and L. Ricciardulli, 2018: The nature of the stochastic wind forcing of ENSO. *J. Climate*, **31**, 8081–8099, https://doi.org/10.1175/JCLI-D-17-0842.1.

Chang, C.-P., J. E. Erickson, and K. M. Lau, 1979: Northeasterly cold surges and near-equatorial disturbances over the winter MONEX area during December 1974. Part I: Synoptic aspects. *Mon. Wea. Rev.*, **107**, 812–829, https://doi.org/10.1175/1520-0493(1979)107<0812:NCSANE>2.0.CO;2.

Chen, D., S. E. Zebiak, A. J. Busalacchi, and M. A. Cane, 1995: An improved procedure for El Niño forecasting: Implications for predictability. *Science*, **269**, 1699–1702, https://doi.org/10.1126/science.269.5231.1699.

——, M. A. Cane, A. Kaplan, S. E. Zebiak, and D. Huang, 2004: Predictability of El Niño over the past 148 years. *Nature*, **428**, 733–736, https://doi.org/10.1038/nature02439.

——, and Coauthors, 2015: Strong influence of westerly wind bursts on El Niño diversity. *Nat. Geosci.*, **8**, 339–345, https://doi.org/10.1038/ngeo2399.

Chen, H.-C., Y.-H. Tseng, Z.-Z. Hu, and R. Ding, 2020: Enhancing the ENSO predictability beyond the spring barrier. *Sci. Rep.*, **10**, 984, https://doi.org/10.1038/s41598-020-57853-7.

Chen, L., T. Li, B. Wang, and L. Wang, 2017: Formation mechanism for 2015/16 Super El Niño. *Sci. Rep.*, **7**, 2975, https://doi.org/10.1038/s41598-017-02926-3.

Chen, M., T. Li, X. Shen, and B. Wu, 2016: Relative roles of dynamic and thermodynamic processes in causing evolution asymmetry between El Niño and La Niña. *J. Climate*, **29**, 2201–2220, https://doi.org/10.1175/JCLI-D-15-0547.1.

Chiodi, A. M., 2019: Diagnosing and predicting ENSO SSTA development from moored-buoy and scatterometer winds. *J. Climate*, **32**, 8755–8770, https://doi.org/10.1175/JCLI-D-19-0183.1.

——, and D. E. Harrison, 2015: Equatorial Pacific easterly wind surges and the onset of La Niña events. *J. Climate*, **28**, 776–792, https://doi.org/10.1175/JCLI-D-14-00227.1.

——, ——, and G. A. Vecchi, 2014: Subseasonal atmospheric variability and El Niño waveguide warming: Observed effects of the Madden–Julian Oscillation and westerly wind events. *J. Climate*, **27**, 3619–3642, https://doi.org/10.1175/JCLI-D-13-00547.1.

Clarke, A. J., and S. V. Gorder, 2003: Improving El Niño prediction using a space-time integration of Indo-Pacific winds and equatorial Pacific upper ocean heat content. *Geophys. Res. Lett.*, **30**, 1399, https://doi.org/10.1029/2002GL016673.

Dee, D. P., and Coauthors, 2011: The ERA-Interim reanalysis: Configuration and performance of the data assimilation system. *Quart. J. Roy. Meteor. Soc.*, **137**, 553–597, https://doi.org/10.1002/qj.828.

Dommenget, D., T. Bayr, and C. Frauen, 2013: Analysis of the non-linearity in the pattern and time evolution of El Niño southern oscillation. *Climate Dyn.*, **40**, 2825–2847, https://doi.org/10.1007/s00382-012-1475-0.

Eisenman, I., L. Yu, and E. Tziperman, 2005: Westerly wind bursts: ENSO's tail rather than the dog? *J. Climate*, **18**, 5224–5238, https://doi.org/10.1175/JCLI3588.1.

Fang, S.-W., and J.-Y. Yu, 2020: Contrasting transition complexity between El Niño and La Niña: Observations and CMIP5/6 models. *Geophys. Res. Lett.*, **47**, e2020GL088926, https://doi.org/10.1029/2020GL088926.

Fang, X.-H., and M. Mu, 2018: Both air-sea components are crucial for El Niño forecast from boreal spring. *Sci. Rep.*, **8**, 10501, https://doi.org/10.1038/s41598-018-28964-z.

Fedorov, A. V., S. Hu, M. Lengaigne, and E. Guilyardi, 2015: The impact of westerly wind bursts and ocean initial state on the development, and diversity of El Niño events. *Climate Dyn.*, **44**, 1381–1401, https://doi.org/10.1007/s00382-014-2126-4.

Gebbie, G., I. Eisenman, A. Wittenberg, and E. Tziperman, 2007: Modulation of westerly wind bursts by sea surface temperature: A semistochastic feedback for ENSO. *J. Atmos. Sci.*, **64**, 3281–3295, https://doi.org/10.1175/JAS4029.1.

Geng, X., W. Zhang, M. F. Stuecker, and F.-F. Jin, 2017: Strong sub-seasonal wintertime cooling over East Asia and Northern Europe associated with super El Niño events. *Sci. Rep.*, **7**, 3770, https://doi.org/10.1038/s41598-017-03977-2.

Goswami, B. N., and J. Shukla, 1991: Predictability of a coupled ocean-atmosphere model. *J. Climate*, **4**, 3–22, https://doi.org/10.1175/1520-0442(1991)004<0003:POACOA>2.0.CO;2.

Guilyardi, E., and Coauthors, 2004: Representing El Niño in coupled ocean–atmosphere GCMs: The dominant role of the atmospheric component. *J. Climate*, **17**, 4623–4629, https://doi.org/10.1175/JCLI-3260.1.

Harrison, D. E., and B. S. Giese, 1991: Episodes of surface westerly winds as observed from islands in the western tropical Pacific. *J. Geophys. Res.*, **96**, 3221–3237, https://doi.org/10.1029/90JC01775.

——, and G. A. Vecchi, 1997: Westerly wind events in the tropical Pacific, 1986–95. *J. Climate*, **10**, 3131–3156, https://doi.org/10.1175/1520-0442(1997)010<3131:WWEITT>2.0.CO;2.

Hartten, L. M., 1996: Synoptic settings of westerly wind bursts. *J. Geophys. Res.*, **101**, 16997–17019, https://doi.org/10.1029/96JD00030.

Hayashi, M., and M. Watanabe, 2016: Asymmetry of westerly and easterly wind events: Observational evidence. *SOLA*, **12**, 42–45, https://doi.org/10.2151/sola.2016-009.

Hendon, H. H., E. Lim, G. Wang, O. Alves, and D. Hudson, 2009: Prospects for predicting two flavors of El Niño. *Geophys. Res. Lett.*, **36**, L19713, https://doi.org/10.1029/2009GL040100.

Hoell, A., M. Hoerling, J. Eischeid, K. Wolter, R. Dole, J. Perlwitz, T. Xu, and L. Cheng, 2016: Does El Niño intensity matter for California precipitation? *Geophys. Res. Lett.*, **43**, 819–825, https://doi.org/10.1002/2015GL067102.

Horii, T., I. Ueki, and K. Hanawa, 2012: Breakdown of ENSO predictors in the 2000s: Decadal changes of recharge/discharge-SST phase relation and atmospheric intraseasonal forcing. *Geophys. Res. Lett.*, **39**, 10707, https://doi.org/10.1029/2012GL051740.

Izumo, T., M. Lengaigne, J. Vialard, I. Suresh, and Y. Planton, 2019: On the physical interpretation of the lead relation between warm water volume and the El Niño Southern Oscillation. *Climate Dyn.*, **52**, 2923–2942, https://doi.org/10.1007/s00382-018-4313-1.

Jin, F.-F., 1997a: An equatorial ocean recharge paradigm for ENSO. Part I: Conceptual model. *J. Atmos. Sci.*, **54**, 811–829, https://doi.org/10.1175/1520-0469(1997)054<0811:AEORPF>2.0.CO;2.

——, 1997b: An equatorial ocean recharge paradigm for ENSO. Part II: A stripped-down coupled model. *J. Atmos. Sci.*, **54**, 830–847, https://doi.org/10.1175/1520-0469(1997)054<0830:AEORPF>2.0.CO;2.

——, S.-I. An, A. Timmermann, and J. Zhao, 2003: Strong El Niño events and nonlinear dynamical heating. *Geophys. Res. Lett.*, **30**, 1120, https://doi.org/10.1029/2002GL016356.

——, S. T. Kim, and L. Bejarano, 2006: A coupled-stability index for ENSO. *Geophys. Res. Lett.*, **33**, L23708, https://doi.org/10.1029/2006GL027221.

——, L. Lin, A. Timmermann, and J. Zhao, 2007: Ensemble-mean dynamics of the ENSO recharge oscillator under state-dependent stochastic forcing. *Geophys. Res. Lett.*, **34**, L03807, https://doi.org/10.1029/2006GL027372.

Keen, R. A., 1982: The role of cross-equatorial tropical cyclone pairs in the Southern Oscillation. *Mon. Wea. Rev.*, **110**, 1405–1416, https://doi.org/10.1175/1520-0493(1982)110<1405:TROCET>2.0.CO;2.

Kessler, W. S., 2002: Is ENSO a cycle or a series of events? *Geophys. Res. Lett.*, **29**, 2125, https://doi.org/10.1029/2002GL015924.

Kleeman, R., and A. M. Moore, 1997: A theory for the limitation of ENSO predictability due to stochastic atmospheric transients. *J. Atmos. Sci.*, **54**, 753–767, https://doi.org/10.1175/1520-0469(1997)054<0753:ATFTLO>2.0.CO;2.

Lai, A. W.-C., M. Herzog, and H.-F. Graf, 2015: Two key parameters for the El Niño continuum: Zonal wind anomalies and western Pacific subsurface potential temperature. *Climate Dyn.*, **45**, 3461–3480, https://doi.org/10.1007/s00382-015-2550-0.

——, ——, and ——, 2018: ENSO forecasts near the spring predictability barrier and possible reasons for the recently reduced predictability. *J. Climate*, **31**, 815–838, https://doi.org/10.1175/JCLI-D-17-0180.1.

Lander, M. A., 1990: Evolution of the cloud pattern during the formation of tropical cyclone twins symmetrical with respect to the equator. *Mon. Wea. Rev.*, **118**, 1194–1202, https://doi.org/10.1175/1520-0493(1990)118<1194:EOTCPD>2.0.CO;2.

Larkin, N. K., and D. E. Harrison, 2002: ENSO warm (El Niño) and cold (La Niña) event life cycles: Ocean surface anomaly patterns, their symmetries, asymmetries, and implications. *J. Climate*, **15**, 1118–1140, https://doi.org/10.1175/1520-0442(2002)015<1118:EWENOA>2.0.CO;2.

Latif, M., and Coauthors, 1998: A review of the predictability and prediction of ENSO. *J. Geophys. Res.*, **103**, 14 375–14 393, https://doi.org/10.1029/97JC03413.

Lengaigne, M., J.-P. Boulanger, C. Menkes, G. Madec, P. Delecluse, E. Guilyardi, and J. Slingo, 2003: The March 1997 westerly wind event and the onset of the 1997/98 El Niño: Understanding the role of the atmospheric response. *J. Climate*, **16**, 3330–3343, https://doi.org/10.1175/1520-0442(2003)016<3330:TMWWEA>2.0.CO;2.

——, ——, ——, P. Delecluse, and J. Slingo, 2004: Westerly wind events in the tropical Pacific and their influence on the coupled ocean-atmosphere system: A review. *Earth's Climate: The Ocean–Atmosphere Interaction, Geophys. Monogr.*, Vol. 147, American Geophysical Union, 49–69.

Lian, T., D. Chen, Y. Tang, and Q. Wu, 2014: Effects of westerly wind bursts on El Niño: A new perspective. *Geophys. Res. Lett.*, **41**, 3522–3527, https://doi.org/10.1002/2014GL059989.

Liang, Y., A. V. Fedorov, and P. Haertel, 2021: Intensification of westerly wind bursts caused by the coupling of the Madden–-Julian Oscillation to SST during El Niño onset and development. *Geophys. Res. Lett.*, **48**, e2020GL089395, https://doi.org/10.1029/2020GL089395.

Love, G., 1985: Cross-equatorial interactions during tropical cyclogenesis. *Mon. Wea. Rev.*, **113**, 1499–1509, https://doi.org/10.1175/1520-0493(1985)113<1499:CEIDTC>2.0.CO;2.

Luther, D. S., D. E. Harrison, and R. A. Knox, 1983: Zonal winds in the central equatorial Pacific and El Niño. *Science*, **222**, 327–330, https://doi.org/10.1126/science.222.4621.327.

Lyon, B., 2004: The strength of El Niño and the spatial extent of tropical drought. *Geophys. Res. Lett.*, **31**, L21204, https://doi.org/10.1029/2004GL020901.

——, and A. G. Barnston, 2005: ENSO and the spatial extent of interannual precipitation extremes in tropical land areas. *J. Climate*, **18**, 5095–5109, https://doi.org/10.1175/JCLI3598.1.

McPhaden, M. J., 2003: Tropical Pacific Ocean heat content variations and ENSO persistence barriers. *Geophys. Res. Lett.*, **30**, 1480, https://doi.org/10.1029/2003GL016872.

——, 2012: A 21st century shift in the relationship between ENSO SST and warm water volume anomalies. *Geophys. Res. Lett.*, **39**, L09706, https://doi.org/10.1029/2012GL051826.

——, and X. Yu, 1999: Equatorial waves and the 1997–98 El Niño. *Geophys. Res. Lett.*, **26**, 2961–2964, https://doi.org/10.1029/1999GL004901.

——, S. E. Zebiak, and M. H. Glantz, 2006: ENSO as an integrating concept in earth science. *Science*, **314**, 1740–1745, https://doi.org/10.1126/science.1132588.

Meinen, C. S., and M. J. McPhaden, 2000: Observations of warm water volume changes in the equatorial Pacific and their relationship to El Niño and La Niña. *J. Climate*, **13**, 3551–3559, https://doi.org/10.1175/1520-0442(2000)013<3551:OOWWVC>2.0.CO;2.

Neale, R. B., J. H. Richter, and M. Jochum, 2008: The impact of convection on ENSO: From a delayed oscillator to a series of events. *J. Climate*, **21**, 5904–5924, https://doi.org/10.1175/2008JCLI2244.1.

Neelin, J. D., D. S. Battisti, A. C. Hirst, F.-F. Jin, Y. Wakata, T. Yamagata, and S. E. Zebiak, 1998: ENSO theory. *J. Geophys. Res.*, **103**, 14 261–14 290, https://doi.org/10.1029/97JC03424.

Nitta, T., 1989: Development of a twin cyclone and westerly bursts during the initial phase of the 1986–87 El Niño. *J. Meteor. Soc. Japan*, **67**, 677–681, https://doi.org/10.2151/jmsj1965.67.4_677.

Ohba, M., and H. Ueda, 2007: An impact of SST anomalies in the Indian Ocean in acceleration of the El Niño to La Niña transition. *J. Meteor. Soc. Japan*, **85**, 335–348, https://doi.org/10.2151/jmsj.85.335.

——, and ——, 2009: Role of nonlinear atmospheric response to SST on the asymmetric transition process of ENSO. *J. Climate*, **22**, 177–192, https://doi.org/10.1175/2008JCLI2334.1.

Okumura, Y. M., and C. Deser, 2010: Asymmetry in the duration of El Niño and La Niña. *J. Climate*, **23**, 5826–5843, https://doi.org/10.1175/2010JCLI3592.1.

Picaut, J., F. Masia, and Y. du Penhoat, 1997: An advective-reflective conceptual model for the oscillatory nature of the ENSO. *Science*, **277**, 663–666, https://doi.org/10.1126/science.277.5326.663.

Planton, Y., J. Vialard, E. Guilyardi, M. Lengaigne, and T. Izumo, 2018: Western Pacific oceanic heat content: A better predictor of La Niña than of El Niño. *Geophys. Res. Lett.*, **45**, 9824–9833, https://doi.org/10.1029/2018GL079341.

Puy, M., J. Vialard, M. Lengaigne, and E. Guilyardi, 2016: Modulation of equatorial Pacific westerly/easterly wind events by the Madden–Julian Oscillation and convectively-coupled Rossby waves. *Climate Dyn.*, **46**, 2155–2178, https://doi.org/10.1007/s00382-015-2695-x.

Rasmusson, E. M., and T. H. Carpenter, 1982: Variations in tropical sea surface temperature and surface wind fields associated with the Southern Oscillation/El Niño. *Mon. Wea. Rev.*, **110**, 354–384, https://doi.org/10.1175/1520-0493(1982)110<0354:VITSST>2.0.CO;2.

Reynolds, R. W., N. A. Rayner, T. M. Smith, D. C. Stokes, and W. Wang, 2002: An improved in situ and satellite SST analysis for climate. *J. Climate*, **15**, 1609–1625, https://doi.org/10.1175/1520-0442(2002)015<1609:AIISAS>2.0.CO;2.

Seiki, A., and Y. N. Takayabu, 2007: Westerly wind bursts and their relationship with intraseasonal variations and ENSO. Part I: Statistics. *Mon. Wea. Rev.*, **135**, 3325–3345, https://doi.org/10.1175/MWR3477.1.

Shi, Y., and J. Su, 2020: A statistical comparison of the westerly wind bursts between the positive and negative phases of the PDO. *J. Meteor. Res.*, **34**, 315–324, https://doi.org/10.1007/s13351-020-9115-9.

Su, J., B. Xiang, B. Wang, and T. Li, 2014: Abrupt termination of the 2012 Pacific warming and its implication on ENSO prediction. *Geophys. Res. Lett.*, **41**, 9058–9064, https://doi.org/10.1002/2014GL062380.

Suarez, M. J., and P. S. Schopf, 1988: A delayed action oscillator for ENSO. *J. Atmos. Sci.*, **45**, 3283–3287, https://doi.org/10.1175/1520-0469(1988)045<3283:ADAOFE>2.0.CO;2.

Timmermann, A., and Coauthors, 2018: El Niño–Southern Oscillation complexity. *Nature*, **559**, 535–545, https://doi.org/10.1038/s41586-018-0252-6.

Tippett, M. K., M. Ranganathan, M. L'Heureux, A. G. Barnston, and T. DelSole, 2019: Assessing probabilistic predictions of ENSO phase and intensity from the North American Multimodel Ensemble. *Climate Dyn.*, **53**, 7497–7518, https://doi.org/10.1007/s00382-017-3721-y.

Tseng, Y., Z.-Z. Hu, R. Ding, and H. Chen, 2017: An ENSO prediction approach based on ocean conditions and ocean–atmosphere coupling. *Climate Dyn.*, **48**, 2025–2044, https://doi.org/10.1007/s00382-016-3188-2.

Tziperman, E., and L. Yu, 2007: Quantifying the dependence of westerly wind bursts on the large-scale tropical Pacific SST. *J. Climate*, **20**, 2760–2768, https://doi.org/10.1175/JCLI4138a.1.

Vecchi, G. A., 2006: The termination of the 1997–98 El Niño. Part II: Mechanisms of atmospheric change. *J. Climate*, **19**, 2647–2664, https://doi.org/10.1175/JCLI3780.1.

——, and D. E. Harrison, 2000: Tropical Pacific sea surface temperature anomalies, El Niño, and equatorial westerly wind events. *J. Climate*, **13**, 1814–1830, https://doi.org/10.1175/1520-0442(2000)013<1814:TPSSTA>2.0.CO;2.

Wallace, J. M., E. M. Rasmusson, T. P. Mitchell, V. E. Kousky, E. S. Sarachik, and H. von Storch, 1998: On the structure and evolution of ENSO-related climate variability in the tropical Pacific: Lessons from TOGA. *J. Geophys. Res.*, **103**, 14 241–14 259, https://doi.org/10.1029/97JC02905.

Wang, W., M. Chen, and A. Kumar, 2010: An assessment of the CFS real-time seasonal forecasts. *Wea. Forecasting*, **25**, 950–969, https://doi.org/10.1175/2010WAF2222345.1.

Watanabe, M., M. Chikira, Y. Imada, and M. Kimoto, 2011: Convective control of ENSO simulated in MIROC. *J. Climate*, **24**, 543–562, https://doi.org/10.1175/2010JCLI3878.1.

Weisberg, R. H., and C. Wang, 1997: A western Pacific oscillator paradigm for the El Niño-Southern Oscillation. *Geophys. Res. Lett.*, **24**, 779–782, https://doi.org/10.1029/97GL00689.

Wyrtki, K., 1975: El Niño—The dynamic response of the equatorial Pacific Ocean to atmospheric forcing. *J. Phys. Oceanogr.*, **5**, 572–584, https://doi.org/10.1175/1520-0485(1975)005<0572:ENTDRO>2.0.CO;2.

Xue, Y., B. Huang, Z.-Z. Hu, A. Kumar, C. Wen, D. Behringer, and S. Nadiga, 2011: An assessment of oceanic variability in the NCEP climate forecast system reanalysis. *Climate Dyn.*, **37**, 2511–2539, https://doi.org/10.1007/s00382-010-0954-4.

Yu, S., and A. V. Fedorov, 2020: The role of westerly wind bursts during different seasons versus ocean heat recharge in the development of extreme El Niño in climate models. *Geophys. Res. Lett.*, **47**, e2020GL088381, https://doi.org/10.1029/2020GL088381.

Zhang, W., J. Li, and F.-F. Jin, 2009: Spatial and temporal features of ENSO meridional scales. *Geophys. Res. Lett.*, **36**, L15605, https://doi.org/10.1029/2009GL038672.

——, S. Li, F.-F. Jin, R. Xie, C. Liu, M. F. Stuecker, and A. Xue, 2019: ENSO regime changes responsible for decadal phase relationship variations between ENSO sea surface temperature and warm water volume. *Geophys. Res. Lett.*, **46**, 7546–7553, https://doi.org/10.1029/2019GL082943.

Zhao, S., F.-F. Jin, and M. F. Stuecker, 2021: Understanding lead times of warm water volumes to ENSO sea surface temperature anomalies. *Geophys. Res. Lett.*, **48**, e2021GL094366, https://doi.org/10.1029/2021GL094366.

Zhu, J., B. Huang, L. Marx, J. L. Kinter, M. A. Balmaseda, R.-H. Zhang, and Z.-Z. Hu, 2012: Ensemble ENSO hindcasts initialized from multiple ocean analyses. *Geophys. Res. Lett.*, **39**, L09602, https://doi.org/10.1029/2012GL051503.

——, A. Kumar, W. Wang, Z.-Z. Hu, B. Huang, and M. A. Balmaseda, 2017: Importance of convective parameterization in ENSO predictions. *Geophys. Res. Lett.*, **44**, 6334–6342, https://doi.org/10.1002/2017GL073669.